NATURAL PRODUCT-BASED ENGINEERING POLYMERS: A SPECIAL EMPHASIS TOWARD DEGRADABLE POLYCARBONATE MATERIALS FROM QUINIC ACID AND CELLULOSE

An Undergraduate Research Scholars Thesis

by

BROOKE A. VERSAW

Submitted to the Undergraduate Research Scholars program at
Texas A&M University
in partial fulfillment of the requirements for the designation as an

UNDERGRADUATE RESEARCH SCHOLAR

Approved by Research Advisor: Dr. Karen L. Wooley

May 2017

Major: Chemistry

TABLE OF CONTENTS

ABSTRACT

Natural Product-based Engineering Polymers: A Special Emphasis Toward Degradable Polycarbonate Materials from Quinic Acid and Cellulose

Brooke A. Versaw
Department of Chemistry
Texas A&M University

Research Advisor: Dr. Karen L. Wooley
Department of Chemistry
Texas A&M University

To address the growing demand for environmentally responsible plastics within and beyond the chemical manufacturing industry, this thesis will examine the synthesis and characterization of a novel class of degradable polycarbonate materials derived from natural precursors and additives. Discussion will first center on the use of solvent-free and light-initiated thiol-ene chemistry towards the fabrication of cross-linked network composites derived from quinic acid and reinforced with cellulose nanocrystals. The focus will then shift to a comparative analysis of these materials designed to ascertain the correlation between increasing cellulose content and bulk thermal and mechanical properties and mechanism of degradation under physiological conditions. These efforts will afford novel bio-based engineering polymer nanocomposites with distinct, tunable thermomechanical properties and resorbable degradation products.

DEDICATION

To Dr. Mildred Cohn, for defying expectations; to Dr. Arnold Beckman, for insisting that excellence is both the highest and the only acceptable standard of work; to my family, for encouraging a lifelong love of learning-I owe you all a tremendous debt of gratitude. Thank you.

ACKNOWLEDGEMENTS

I would first like to thank my advisor, Dr. Karen Wooley, for her guidance and support. Her enthusiasm for polymer chemistry has informed and encouraged my own; her mentorship has made me a better student and a better scientist.

I also wish to recognize the contributions of Wooley Group members Drs. Lauren Link and Samantha Kristufek to the work presented here. Their advice, perspective, and extensive reserves of patience have proven indispensable.

Finally, I gratefully acknowledge the Laboratory for Synthetic-Biologic Interactions at Texas A&M University for instrument access, the Laboratory of Biological Mass Spectroscopy at Texas A&M University for their assistance in procuring mass spectroscopy data, and the Arnold & Mabel Beckman Foundation (Beckman Scholars Program) and National Science Foundation (CHE-1610311) for their generous financial support.

NOMENCLATURE

BDBMA	1,4-butanediol bis(mercaptoacetate)
DCM	dichloromethane
DMA	Dynamic mechanical analysis
DMF	N, N-dimethylformamide
DMPA	2,2-dimethoxy-2-phenylacetophenone
DSC	Differential scanning calorimetry
1,2-EDT	1,2-ethanedithiol
NMR	Nuclear magnetic resonance spectroscopy
MS	Mass spectrometry
TAQA	tris(alloc)quinic acid
TEGBMP	tetraethylene glycol bis(3-mercaptopropionate)
TGA	Thermogravimetric analysis
THF	tetrahydrofuran
TLC	Thin layer chromatography
TMEDA	N,N,N',N'-tetramethylethylenediamine

CHAPTER I

INTRODUCTION

Recent years have witnessed a substantial increase in demand for sustainable plastics. Continued needs for versatile, high-performance materials coupled with heightened scrutiny over rapidly depleting stores of petrochemical resources have prompted substantial corporate, academic, and governmental interest in the synthesis of bio-based polymers that offer a combination of useful mechanical properties and controlled degradation.

In 2009, growing concerns about dependence on petrochemical feedstocks prompted Coca-Cola to introduce a polyethylene terephthalate (PET) soft drink bottle that incorporated up to 30% plant-based renewable materials;[1] in 2015, Lego announced a plan to replace the acrylonitrile-butadiene-styrene blend that constitutes the majority of its signature toy blocks with a plant-based polymer.[2] Most recently, Synvina, a subsidiary of chemical manufacturers BASF and Avantium, has invested heavily in plant facilities and equipment for the production of polyethylenefuranoate (PEF), a food-grade commodity plastic derived from the natural sugar fructose.[3] These initiatives constitute significant outlays of both physical assets and human research and development potential, indicating that alternative plastics represent not a niche market, but a rising industry standard.

The transition from petroleum-based materials to their naturally-derived counterparts is equally prominent in medicine. In particular, natural product-based materials have offered tangible progress towards a prominent issue facing the field of orthopedics: patient-device fit in surgical

orthopedic implants. Orthopedic injuries represent a substantial fraction of annual emergency room visits, with incidence rates of 210.4/10,000 patients/year and 160.0/10,000 patients/year reported for males and females, respectively.[4] Prescribed treatments vary according to the severity of the injury. For relatively minor breaks, external fixation by brace or cast may suffice. More extensive injuries frequently require surgical intervention through placement of a removable implant-a pin or screw designed to stabilize and align the bones during the healing process.[5]

Surgical-grade steel, a current standard of care, has demonstrated two key limitations to successful implementation. With a storage modulus (E`) of approximately 200 GPa, steel is substantially tougher than cortical bone (17-24 GPa) and cancellous bone (0.1-4.5 GPa).[6] This disparity in mechanical properties contributes to the phenomenon of stress shielding, in which the metal implant bears the full weight of mechanical stress normally allocated to the surrounding bone, limiting osteoblast activity and therefore delaying bone formation and the healing process.[5] Placement of steel implants also necessitates a subsequent removal surgery, which may contribute to further delays in healing.

Recently, poly(lactic acid) (PLA), a naturally-derived polymer synthesized from the cyclic diester L-lactide, has gained prominence as a bio-based alternative to conventional steel materials, most notably for treatment of orbital floor fractures.[7-8] With a Young's modulus comparable to cancellous bone[6] and degradation possible under physiological conditions, PLA-based implants offer a promising treatment option for orthopedic injuries requiring internal fixation.

In both industrial campaigns and clinical practices, naturally-derived, nontoxic, and ultimately degradable polymers offer a promising combination of mechanical properties and controlled degradation. Moreover, these materials increasingly rival their petrochemical counterparts in both scope and functionality.[9] Recent studies have reported a diverse array of polymers synthesized from readily available natural product building blocks that demonstrate physical properties (*e.g.,* glass transition temperatures, storage moduli, and optical clarity) comparable or even superior to those of petroleum-based standards.[10-11] These materials include polycarbonates derived from limonene,[11] poly(carbonate amides) from ferulic acid and tyrosine,[12] polyesters from *D*-galactose and other saccharides,[13] epoxy resins from quercetin,[14] and cross-linked networks from quinic acid.[10] To expand this growing library, a novel class of polymeric nanocomposite materials was developed.

Through solvent-free and light-initiated processes, composite materials were fabricated from a copolymer of quinic acid, a chlorogenic acid found in coffee, tea, and green vegetables,[15] and cellulose, a polysaccharide and major component of plant matter. Previous studies identified quinic acid as a natural precursor in the design of linear[16] and cross-linked[10] biodegradable polycarbonate materials with tunable thermal and mechanical properties. To expand the range of achievable properties for these materials while maintaining both their natural product origins and benign degradation, composites integrated with nanocrystals of cellulose were fabricated and their glass transition and degradation temperatures (T_g and T_d, respectively) and storage moduli (E`) measured to assess the influence of varying percentages of cellulose additive on thermomechanical properties and degradation time.

CHAPTER II

METHODS

Materials & characterization

Materials

Acetonitrile (Sure-Seal), Amberlyst ion-exchange resin, allyl chloroformate, cellulose microcrystals (20 μm), 2,2-dimethoxy-2-phenylacetone (DMPA), 1,2-ethanedithiol (EDT), quinic acid, N,N,N',N'-tetramethylethylenediamine (TMEDA), *tert*-butyldimethylsilylchloride (TBDMSCl), and tyrosol were obtained from Sigma Aldrich. 1,4-butanediol bis(mercaptoacetate) and tetraethylene glycol bis(3-mercaptopropionate) were purchased from Wako Chemical. Sodium hydride (NaH, 60% dispersion in mineral oil) was obtained from Acros Organic. Silver fluoride (AgF) and imidazole were purchased from Alfa Aesar. Anhydrous dimethylformamide (DMF) and tetrahydrofuran (THF) were obtained by in-house solvent purification system (SPS).

Characterization

^{1}H and ^{13}C nuclear magnetic resonance (NMR) spectra were obtained on a Mercury 300 spectrometer interfaced to a UNIX computer with VnmrJ software. Chemical shifts were referenced to the appropriate solvent (CD_3OD: 3.31, $CDCl_3$: 7.26 ppm). Infrared (IR) spectra were obtained on a Shimadzu IR Prestige system and analyzed by IResolution software. Thermogravimetric analysis (TGA) was performed on a Mettler Toledo TGA/DSC 1 and analyzed using Mettler STARe software. Samples were heated under argon (40 mL/min) from 25-400 °C at 10 °C/minute. Differential scanning calorimetry (DSC) was performed on a

Mettler Toledo DSC 1 with a heating rate of 10 °C/minute and analyzed by Mettler STARe software. Glass transition temperatures were recorded as the midpoint of the inflection tangent of the third heating cycle. Dynamic mechanical analysis (DMA) was performed on a Mettler Toledo TT-DMA system in the compression mode. Samples were sanded with 600 grit sandpaper and subjected to sinusoidal compression with a frequency of 1 Hz and static to dynamic force ratio of 1.5 from -30 to 120 °C at a rate of 2 °C/minute. Data were collected using Triton Laboratory software at 10 s intervals and exported to Origin Pro 10.0 software.

Methods

Lactonization of quinic acid[17]

Quinic acid (14.96 g, 77.86 mmol), Amberlyst resin, DMF (37.5 mL), and benzene (140 mL) were combined in a 250 mL round-bottom flask outfitted with a stir bar and connected to a Dean-Stark trap and condenser. The reaction mixture was heated to 145 °C, stirring constantly, and was heated at reflux for 18 hours, monitored by thin layer chromatography (TLC). Once cooled to room temperature, the reaction mixture was filtered with methanol. The colorless filtrate was concentrated by rotary evaporation to afford a white crystalline solid, which was combined with 75 mL of hexanes and 35 mL of dichloromethane (DCM) and stirred overnight. Filtration with DCM afforded the lactone of quinic acid in good yield (12.97 g, 96% yield). ^{1}H NMR (CD_3OD, 300 MHz): δ 4.71-4.67 ppm (t, J=4.7, 1 H, H-3), 3.99-3.95 ppm (t, 1 H, H-4), 3.71-3.67 ppm (m, 1 H, H-5), 2.48-2.44 ppm (d, J=2.5, 1 H, H-2), 2.24-2.19 ppm (m, 1 H, H-2), 2.03-1.99 ppm (m, 1 H, H-6), 1.90-1.82 ppm (t, J=1.9, 1 H, H-6). ^{13}C NMR (CD_3OD, 125 MHz): δ 178.0 ppm (C7) 76.5 ppm (C1), 71.7 ppm (C5), 65.9 ppm (C4), 65.4 ppm (C3), 38.7 ppm (C2), 36.4 ppm (C6); FTIR (neat, cm^{-1}): 3524, 3509, 3331, 1678, 1265, 1223, 1134, 1064.

Synthesis of tris(alloc)quinic acid (TAQA)[10]

Quinic acid lactone (7.38 g, 42.4 mmol) was added to an oven-dried 500 mL round-bottom flask equipped with 3A molecular sieves and a stir bar. The flask was purged and placed under nitrogen, and 140 mL of DCM were added. The flask was cooled to -4 °C; N,N,N',N'-tetramethylethylenediamine (TMEDA, 26.1 g, 174 mmol) was then added. The reactants were stirred for 20 minutes. Addition of allyl chloroformate (32.0 mL, 301 mmol, diluted in 12 mL DCM) proceeded in a dropwise fashion over 60 minutes. The reaction was allowed to proceed for 16 hours, monitored by TLC. The reaction mixture was filtered with DCM; the colorless filtrate was then washed twice with 350 mL of distilled water and once with 350 mL of a solution of $CuSO_4$ (10 % w/w). The organic layers were combined and concentrated to a brown oil, then purified by flash column chromatography (3:1 hexanes: ethyl acetate) and concentrated to afford TAQA as a colorless, highly viscous oil (11.7 g, 65% yield). ^{1}H NMR ($CDCl_3$, 300 MHz): δ 6.00-5.86 ppm (m, 1 H, H-10), 5.42-5.39 ppm (m, 1 H, H-4), 5.38-5.23 ppm (m, 1 H, H-11), 5.03-4.98 ppm (m, 1 H, H-5), 4.93 ppm (dd, J=6.0, 5.0, 1-H, H-3), 4.65-4.60 ppm (m, 1 H, H-9), 3.22-3.14 ppm (m, 1 H, H-2), 2.56-2.52 ppm (d, J=6.0, 1 H, H-2), 2.41-2.28 ppm (m, 2 H, H-6). ^{13}C NMR ($CDCl_3$, 125 MHz): δ 170.4 ppm (C7), 153.7 ppm, (C8), 153.2 ppm (C8), 131.1 ppm (C10), 130.7 ppm (C10), 119.7 ppm (C11), 119.6 ppm (C11), 77.3 ppm (C1), 76.7 ppm (C1), 73.2 ppm (C3), 69.1 ppm (C9), 67.7 ppm (C4), 33.3 ppm (C2); FTIR (neat, cm^{-1}): 2981, 1808, 1748, 1231, 990, 935.

Extraction of cellulose nanocrystals from cellulose microcrystals[18]

Cellulose microcrystals (2.00 g) were suspended in 40 mL of deionized water and sonicated for six hours. The supernatant liquid was decanted, frozen, and then lyophilized for 72 hours to

afford cellulose nanocrystals (0.791 g, 40% yield, nanoparticle concentration of 19.8 mg/mL in solution).

General procedure for the fabrication of poly(thioether-co-carbonate) neat films

Resins were prepared by combining TAQA and a multifunctional thiol crosslinker to afford equimolar ratios of functional groups. TAQA and thiol crosslinker were first blended by vortexing; to this mixture, 2,2-dimethoxy-2-phenylacetophenone (DMPA, 1 wt% for all resins) was added. The resin was vortexed again until DMPA was fully dissolved. The mixture was then cast in a mold composed of glass slides separated by stacked glass spacers to afford a film of approximate thickness 0.3 mm. The resin was cured on a Fusion curing belt (speed=1 m/min, 10 passes). The cured film was then separated from the glass mold and post-cured under vacuum at 120°C for 24 hours.

General procedure for the fabrication of poly(thioether-co-carbonate) cellulose nanocomposite films

To prepare cellulose nanocomposite materials, TAQA monomer and a multifunctional thiol crosslinker were combined by equal molar ratios of functional groups and vortexed until thoroughly mixed. To this mixture, nanocrystalline cellulose, prepared as described above, was added. The vial containing the uncured resin was carefully sealed and then placed in a bath sonicator for five minutes. Temperatures of both the bath and the vial containing the resin were carefully monitored to prevent excess exposure to heat or evolution of gas. DMPA (1 wt%) was then added to the resin and vortexed until dissolved. The resin was then cast and cured as described above.

General procedure for the fabrication of poly(thioether-co-carbonate) cellulose nanocomposite pucks

TAQA monomer and a multifunctional thiol crosslinker were combined by equal molar ratios of functional groups and vortexed until thoroughly mixed. To this mixture, nanocrystalline cellulose, prepared as described above, was added. The vial containing the uncured resin was carefully sealed and then placed in a bath sonicator for five minutes. DMPA (1 wt%) was then added to the resin and vortexed until dissolved. Pucks were cast by transferring the uncured resin by pipet to the wells of a silicone puck mold (8 drops per well) coated with Sprayon MR311 dry film release spray. The pucks were then cured in a UV chamber (λ=256 nm) for 30 minutes. Pucks were then released from their molds and cured for an additional 30 minutes, then post-cured under vacuum at 120°C for 24 hours.

Degradation studies of poly(thioether-co-carbonate) cellulose nanocomposite pucks

Samples of 1,2-EDT-*co*-TAQA, TEGBMP-*co*-TAQA, and BDBMA-*co*-TAQA nanocomposites containing 2.5 % cellulose by weight were immersed in 3 mL of phosphate buffered saline (PBS) solution buffered to pH 7.4 and incubated at 37°C. Samples in quintuplicate were removed weekly, rinsed with nanopure water, and massed. After drying under vacuum at 30°C for 72 hours, samples were massed a second time, then returned to fresh PBS solution.

CHAPTER III

RESULTS & DISCUSSION

Poly(thioether-*co*-TAQA) networks

The preparation of poly(thioether-*co*-carbonate) crosslinked networks began with the two-step synthesis of tris(alloc)quinic acid (TAQA), initially reported by Lauren Link, et al. and depicted in **Scheme 1**.[10] Starting from quinic acid (**1**), sequential lactonization (**2**) and functionalization by allyl chloroformate were employed to afford the trifunctional monomer tris(alloc)quinic acid (TAQA, **3**).

Scheme 1. Synthesis of TAQA monomer

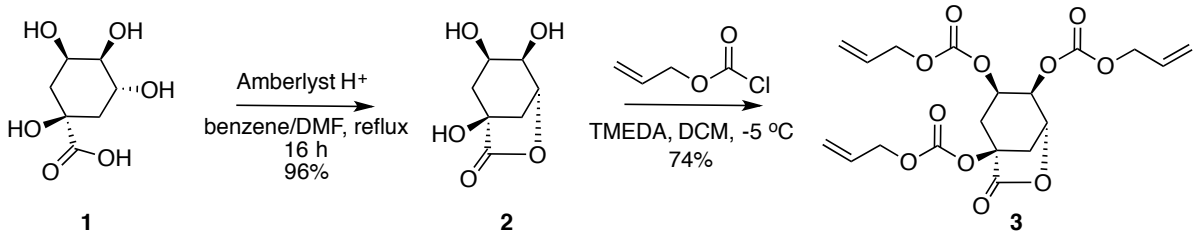

Copolymerization of TAQA with a multifunctional thiol under UV irradiation *via* solvent-free thiol-ene chemistry afforded uniform poly(thioether-*co*-TAQA) cross-linked networks (**4**) with thermal and mechanical properties tunable through variation of the thiol cross-linker, and thus the cross-link density of the resultant materials. A range of di-, tri-, and tetrafunctional thiol crosslinkers of varying chain lengths were utilized to afford a small library of poly(thioether-*co*-TAQA) networks (**Scheme 2**).

Scheme 2. Cross-linking of Poly(thioether-*co*-TAQA) Networks

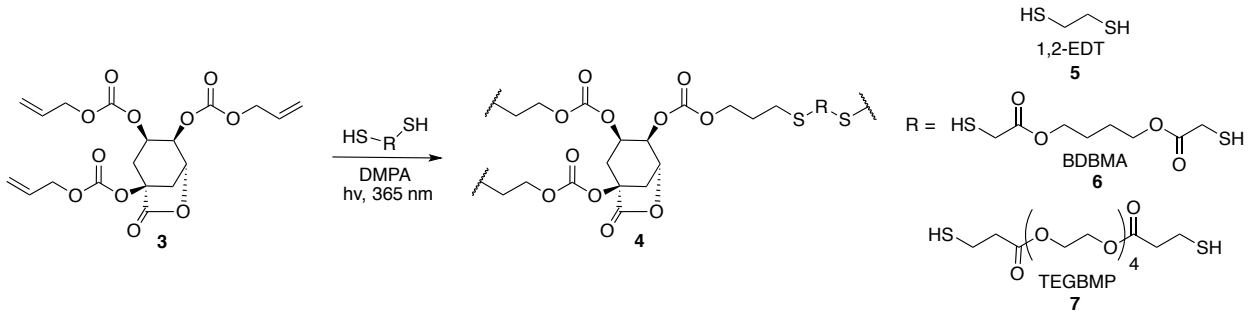

Extended networks are shown in **Schemes 3-6**.

Scheme 3. 1,2-EDT-*co*-TAQA

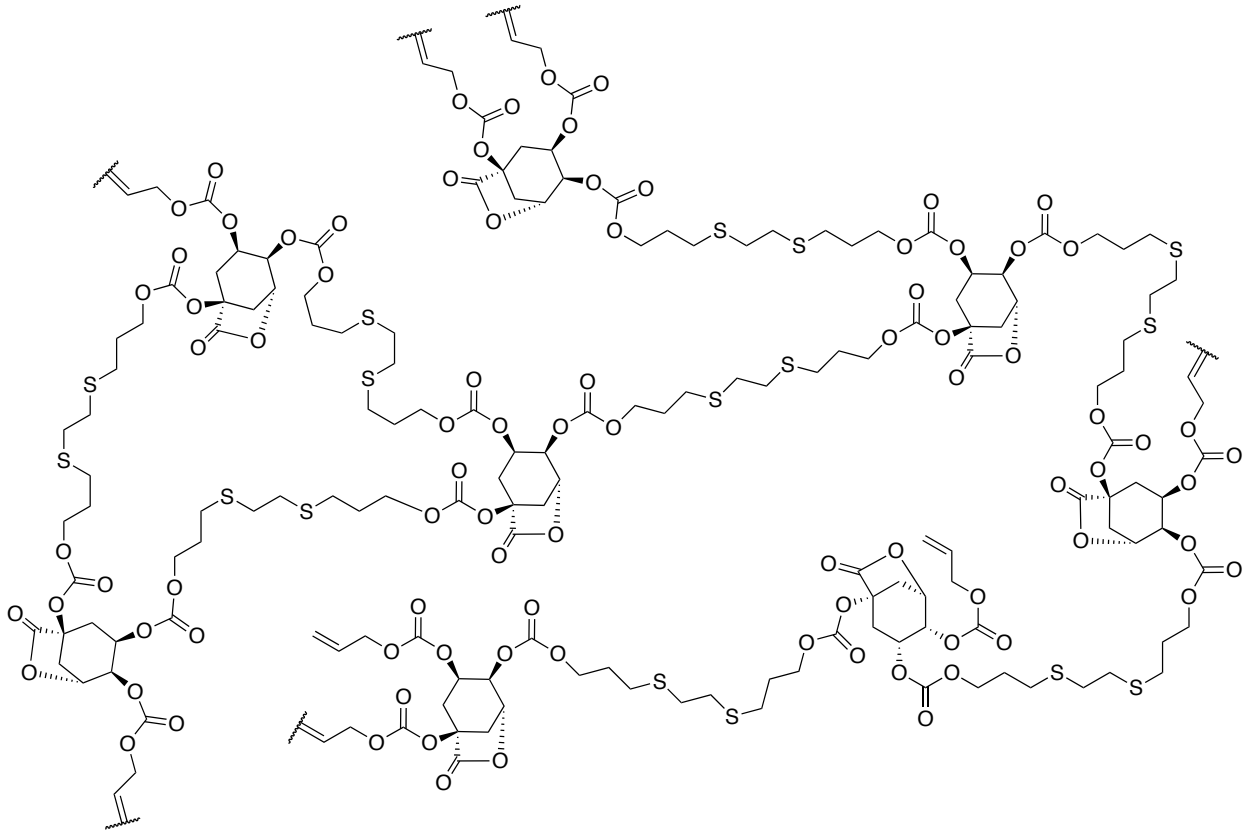

Scheme 4. BDBMA-*co*-TAQA

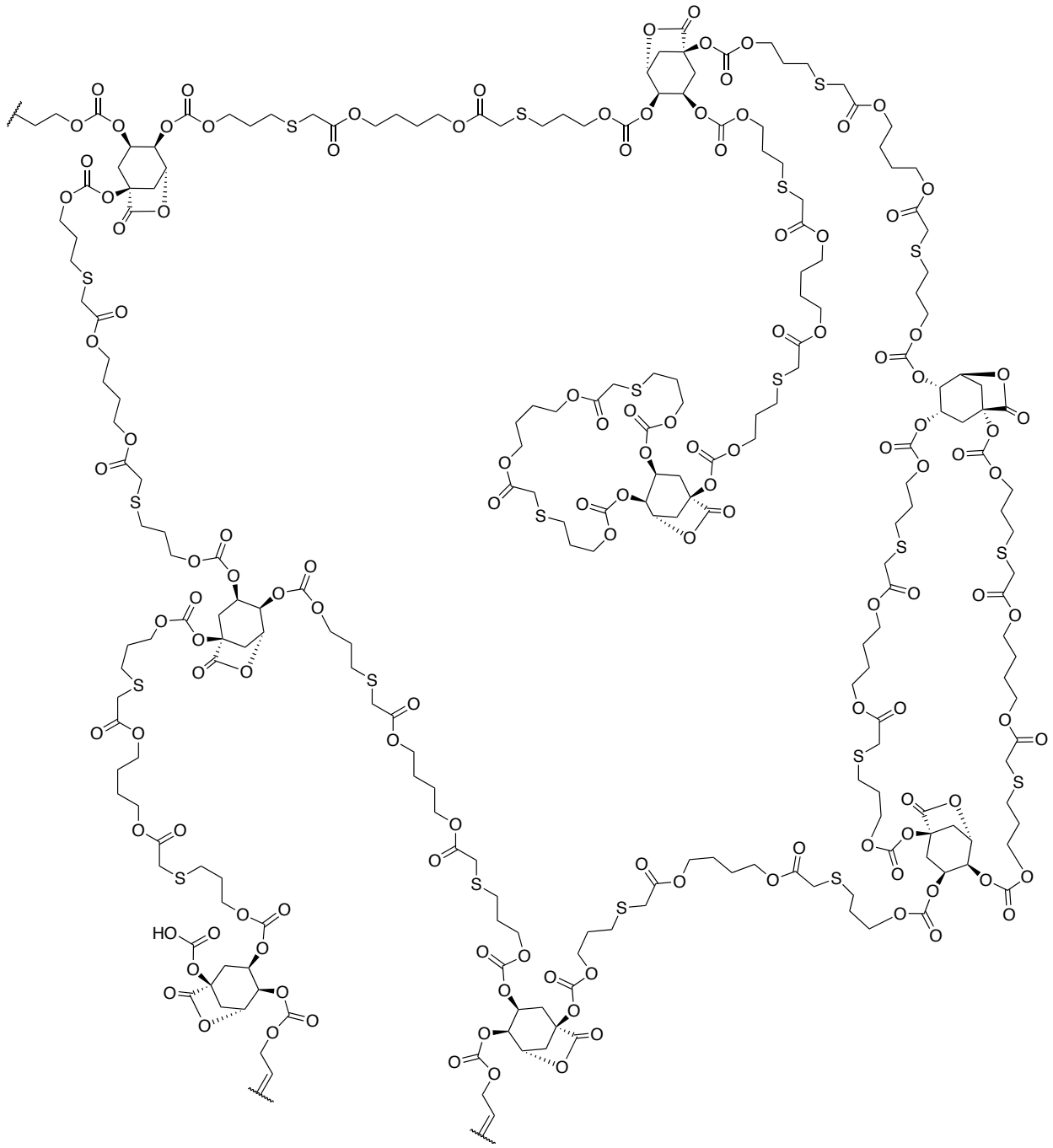

Scheme 5. TEGBMP-*co*-TAQA

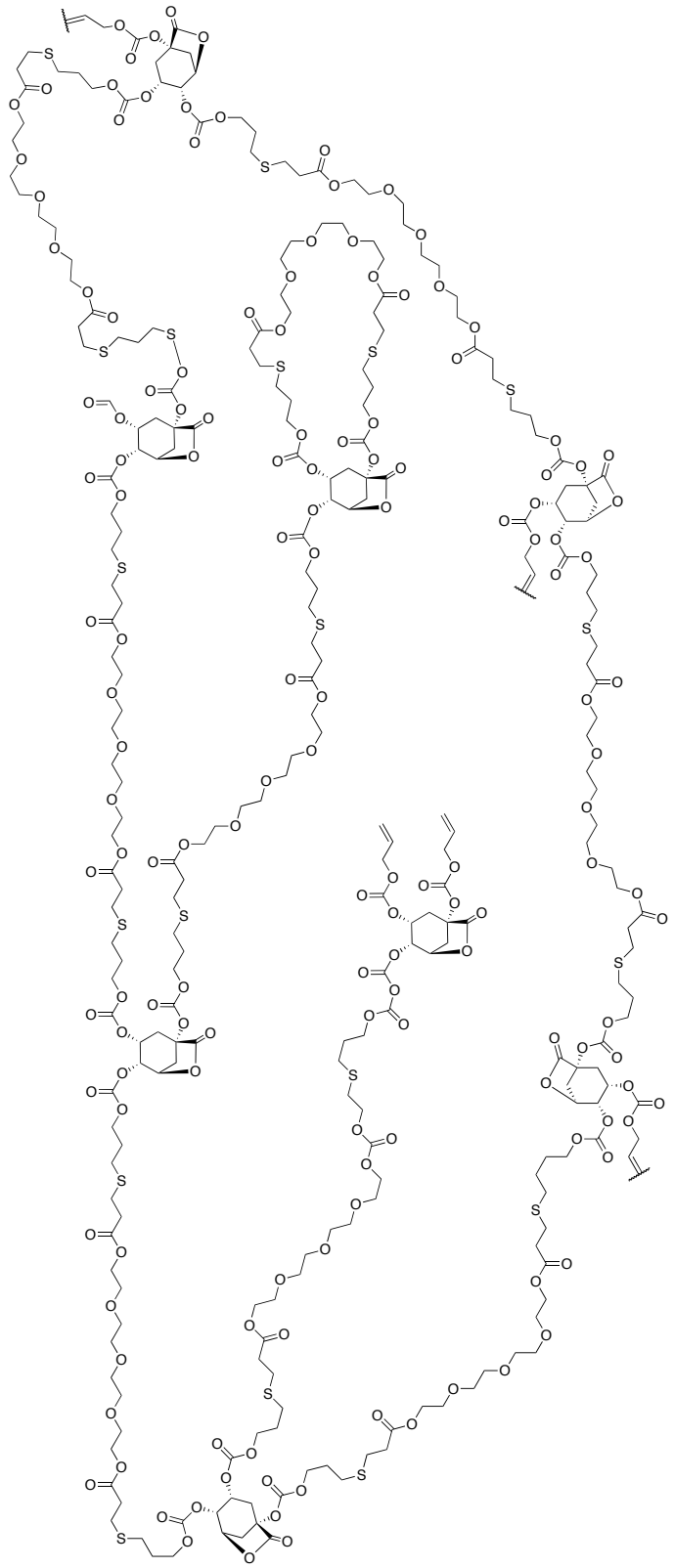

Studies of the material properties of these networks indicated a broad range of achievable glass transition temperatures (T_g, -18 to 65°C) and Young's moduli (E′, 357 to 1440 MPa).[10] A close correlation was noted between the length of the thiol crosslinker employed and the thermomechanical properties of the bulk materials, with short-chain thiols contributing to higher levels of cross-link density and, consequently, higher values for T_g and E′. Of note, the networks also demonstrated degradation under biological conditions, with no cytotoxicity noted for either the cross-linked networks or their degradation products. Degradation timescales ranged from 10 weeks with total mass loss to over 25 weeks with 71.1% mass remaining.[19] To augment the scope of these properties without sacrificing either the natural origins of the materials or their benign degradation profiles, the fabrication of poly(thioether-*co*-TAQA) networks reinforced with neat cellulose nanocrystals was proposed and conducted (**Scheme 6**).

Scheme 6. Crosslinking of Poly(thioether-*co*-TAQA) Network Composites

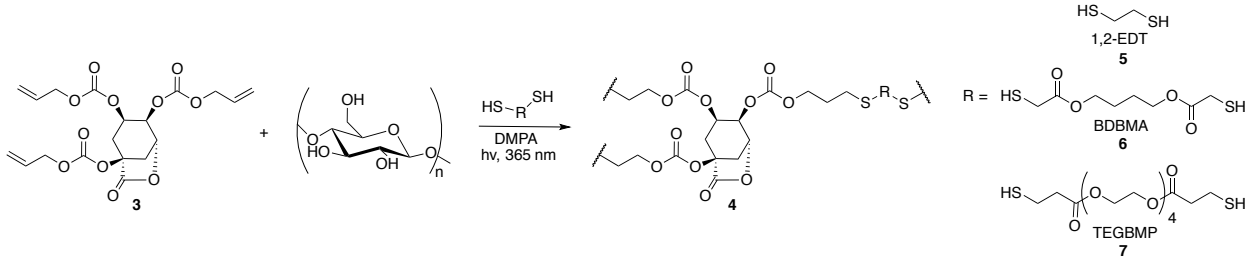

Cellulose, a polysaccharide that constitutes a major structural component of plant matter, was selected as an ideal additive for these materials; it is widely abundant, enjoys FDA status as a Generally Regarded as Safe (GRAS) substance, and is well-established as a mechanical reinforcement agent for polyester-based materials.[20-21] Unmodified nanocrystals were employed to avoid the possibility of chemical interactions between the polymer matrix and side chains present on chemically treated cellulose. To provide an efficient basis for comparison with the cross-link density studies originally conducted, poly(thioether-*co*-TAQA) composites were fabricated using three difunctional thiol crosslinkers of increasing chain length: 1,2-ethanedithiol

(1,2-EDT, **5**), 1,4-butanediol bis(mercaptoacetate) (BDBMA, **6**), and tetraethyleneglycol bis(3-mercaptopropionate) (TEGBMP, **7**).

Optimization of cellulose poly(thioether-*co*-TAQA) nanocomposite fabrication methods

To determine the fabrication method that would maximize both additive loading capacity and quality of dispersion, resins of 1,2-EDT- *co*-TAQA containing 2.5 percent cellulose nanocrystals by weight were blended by either by vortexing or by stirring for five minutes and cast as thin films. Films were chosen as the target bulk form for the optimization study primarily to conserve resin and facilitate rapid, efficient preparation of samples suitable for thermal analysis. EDT was selected as the model crosslinker as it produced the lowest viscosity resin of the three poly(thioether-*co*-TAQA) systems studied. Consequently, fabrication techniques that failed in a low-viscosity medium would not be expected to prevail in high-viscosity resins with greater diffusion-related limitations on dispersion. Quality of dispersion and, by extension, the efficacy of the method selected, was evaluated according to the thermal properties of the resultant materials, as measured by TGA and DSC. After blending of the resin and nanocellulose, photoinitiator was then added to each sample. The resins were then vortexed until thoroughly mixed and immediately cast and cured. As full integration by stirring proved challenging for the 2.5 percent by weight resin mixtures, a subsequent experiment was devised to evaluate bath sonication as an additional technique capable of accommodating higher levels of cellulose incorporation. Consequently, additional 1,2-EDT-*co*-TAQA resins were prepared and blended with 2.5 and 5 percent cellulose nanocrystals by weight either by vortexing, as examined previously, or by bath sonication for a duration of five minutes. The thermal properties obtained for the materials fabricated are reported below in **Table 1.**

Table 1. Optimization of fabrication methods for poly(thioether-*co*-TAQA) nanocomposites

Cellulose content (% by weight)	Fabrication method	T_g (°C)	T_d (°C)
2.5	Stirring	69	251
2.5	Vortexing	70	255
2.5	Sonication	71	251
5.0	Vortexing	70	260
5.0	Sonication	75	263

At intermediate (2.5% by weight) levels of additive content, the method of fabrication appeared less significant, as integration of cellulose nanocrystals by stirring and by vortexing afforded composite films with comparable glass transition temperatures. However, the importance of careful method selection became more pronounced at higher additive concentrations, as films fabricated by sonication demonstrated glass transition temperatures significantly higher than those fabricated by vortexing.

Thermal and mechanical analysis of cellulose poly(thioether-*co*-TAQA) nanocomposites

With the optimized methods for composite fabrication in hand, a thorough investigation of the correlations between cellulose content and thermomechanical properties was completed. Resins of 1,2-EDT-*co*-TAQA, BDBMA-*co*-TAQA, and TEGBMP-*co*-TAQA containing up to 7.5 percent cellulose nanocrystals by weight were formulated according to the procedures developed in the optimization experiments, drop-cast, and cured in silicone molds to afford cylindrical pucks. Pucks were selected over films for the bulk form in this analysis in order to facilitate dynamic mechanical analysis (DMA) measurements in compression mode, which would afford a more realistic approximation of the weight-bearing stress experienced by an orthopedic implant.

those fabricated by vortexing.

Thermal analysis

Samples were analyzed first by TGA, and then by DSC to assess T_d and T_g, respectively. As the addition of cellulose nanocrystals was not expected to influence crosslinking, values of T_d were anticipated to remain relatively constant across all samples fabricated with the same thiol crosslinker, regardless of additive content. In contrast, as the cellulose nanocrystals were intended to reinforce the crosslinked networks, values of T_g were expected to increase with increasing levels of additive content. Results of these analyses are reported in **Table 2,** depicted below.

Table 2. Thermal properties of cellulose poly(thioether-*co*-TAQA) nanocomposites

Network Type	Cellulose Content (% by weight)	T_g (°C)	T_d (°C)
TEGBMP-*co*-TAQA	0	-15	264
TEGBMP-*co*-TAQA	0.5	-8	271
TEGBMP-*co*-TAQA	1.0	-4	279
TEGBMP-*co*-TAQA	2.5	-7	281
TEGBMP-*co*-TAQA	5.0	-8	281
TEGBMP-*co*-TAQA	7.5	-2	287
BDBMA-*co*-TAQA	0	12	304
BDBMA-*co*-TAQA	0.5	10	303
BDBMA-*co*-TAQA	1.0	11	305
BDBMA-*co*-TAQA	2.5	16	303
BDBMA-*co*-TAQA	5.0	16	304
BDBMA-*co*-TAQA	7.5	15	305
1,2-EDT-*co*-TAQA	0	54	259
1,2-EDT-*co*-TAQA	0.5	54	263
1,2-EDT-*co*-TAQA	1.0	52	264
1,2-EDT-*co*-TAQA	2.5	54	257
1,2-EDT-*co*-TAQA	5.0	50	258
1,2-EDT-*co*-TAQA	7.5	56	259

Overall, the hypotheses prepared were supported by the data collected. The composite materials demonstrated only minor variations in T_d from the values recorded for the unmodified crosslinked networks, even at high percentages of additive content, significant increases in T_g

with increasing crosslink density, and modest increases in T_g up to 11°C with increasing cellulose content. These trends are summarized in **Figure 1.**

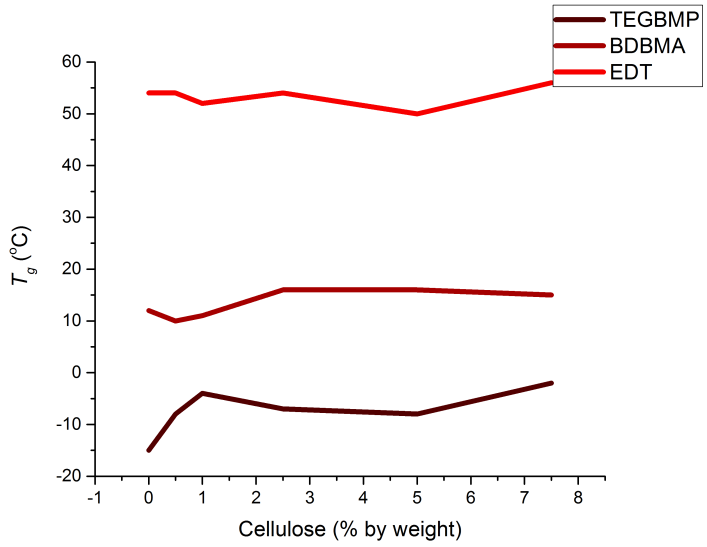

Figure 1. Change in T_g with increasing cellulose content

Of note, the overall range of glass transition temperatures measured was approximately 10°C lower than that obtained in the optimization study. This was to be expected, as the samples prepared for this analysis were cured in a UV chamber, rather than a curing belt, to accommodate the three-dimensional nature of the samples. As the UV chamber employs a less intense light source, materials with lower glass transition temperatures were afforded. Gains in T_g afforded by the addition of cellulose nanocrystals varied between levels of additive concentration. This variation, which indicates incomplete or uneven additive dispersion, likely arose from aggregation of the cellulose nanocrystals induced by a mismatch in miscibility between the hydrophobic polymer matrix and hydrophilic moieties on the unmodified cellulose additive. orthopedic implant.

Mechanical analysis

Aggregation may again be employed to explain the correlation between cellulose content and mechanical properties. To assess the mechanical performance of the nanocomposite materials, measurements of the storage modulus (E′) were performed in compression mode. The results of these experiments are compiled in **Table 3**.

Table 3. Mechanical properties of cellulose poly(thioether-*co*-TAQA) nanocomposites.

Network Type	Cellulose Content (% by weight)	Storage Modulus (MPa)
TEGBMP-*co*-TAQA	0	81
TEGBMP-*co*-TAQA	0.5	104
TEGBMP-*co*-TAQA	1.0	211
TEGBMP-*co*-TAQA	2.5	125
TEGBMP-*co*-TAQA	5.0	196
TEGBMP-*co*-TAQA	7.5	101
BDBMA-*co*-TAQA	0	132
BDBMA-*co*-TAQA	0.5	238
BDBMA-*co*-TAQA	1.0	80
BDBMA-*co*-TAQA	2.5	158
BDBMA-*co*-TAQA	5.0	176
BDBMA-*co*-TAQA	7.5	57
1,2-EDT-*co*-TAQA	0	73
1,2-EDT-*co*-TAQA	0.5	37
1,2-EDT-*co*-TAQA	1.0	72
1,2-EDT-*co*-TAQA	2.5	34
1,2-EDT-*co*-TAQA	5.0	36
1,2-EDT-*co*-TAQA	7.5	53

As with the glass transition temperatures, it was anticipated that cellulose would uniformly provide mechanical reinforcement to the underlying cross-linked networks, manifested by an increase in storage modulus proportional to the amount of nanocrystals added. However, the results obtained from DMA testing indicated that the extent of this modulation of properties varies widely between poly(thioether-*co*-TAQA) resins. These trends are summarized in **Figure 2**.

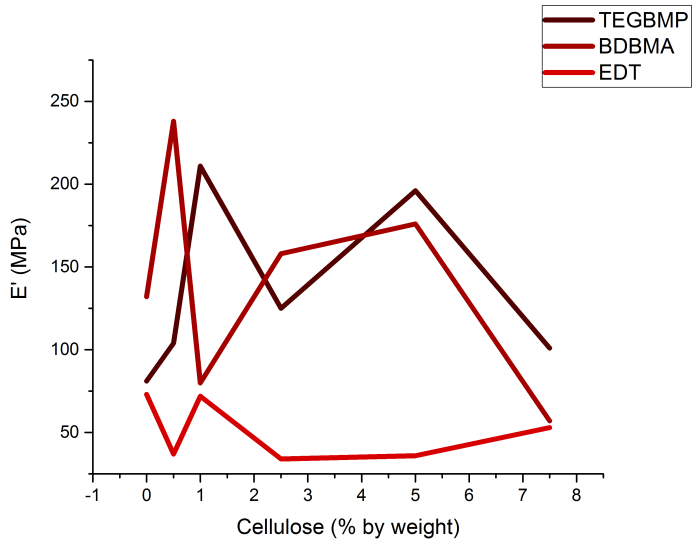

Figure 2. Change in modulus with increasing cellulose content

The TEGBMP-*co*-TAQA and BDBMA-*co*-TAQA nanocomposites demonstrated an almost twofold increase in storage modulus over the unmodified networks with integration of 0.5 and 1.0 percent cellulose by weight, respectively. However, the 1,2-EDT-*co*-TAQA composites realized almost no gains in storage modulus and appeared to decline in mechanical strength at high levels of additive content. These trends did not appear to result from uneven curing as a product of the relative viscosities of the uncured resins, as the 1,2-EDT-*co*-TAQA composite resins, which experienced the lowest gains in modulus, were the least viscous of the three systems tested. Rather, they may again be attributed to the tendency of cellulose to aggregate in the polymer substrate during the fabrication process, creating structural inconsistencies in the cured composite networks that would in turn result in an irregular response to the application of mechanical stress.

Significance of thermal and mechanical analysis

The broader implications of these thermal data are perhaps best understood in the context of their potential applications. **Figure 3** summarizes the highest values of T_g achievable by the 1,2-EDT-, BDBMA-, and TEGBMP-*co*-TAQA nanocomposites alongside the average homeostatic temperature of the human body.[22]

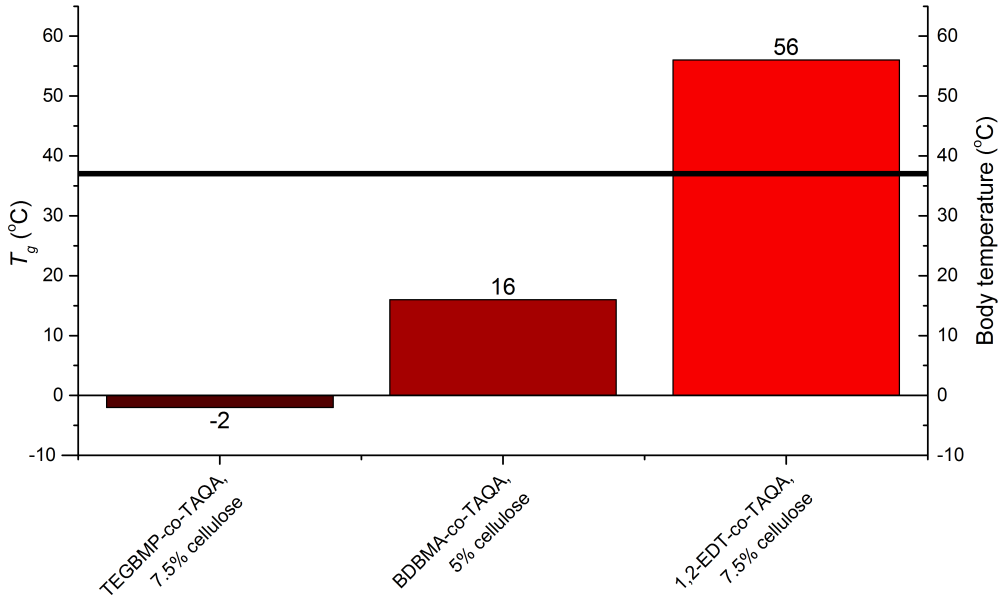

Figure 3. Comparison of T_g of poly(thioether-*co*-TAQA) composites with respect to human body temperature

The glass transition temperatures of the TEGBMP-*co*-TAQA, BDBMA-*co*-TAQA, and 1,2-EDT-*co*-TAQA nanocomposites occur above and below physiologically relevant temperatures; this indicates that the materials will maintain in the human body the solid state that they occupy at room temperature. The elastomeric TEGBMP- and BDBMA-based composites will remain in the rubbery state; the thermoset 1,2-EDT-*co*-TAQA composites will remain in the glassy state.

This consistency is critical for continuity of device performance, as an *in vivo* transition from glassy to rubbery states could result in significant changes in the toughness and flexibility of the materials and potential device failure. The mechanical properties may be considered in a similar fashion. **Table 4** reports the maximum values of E` obtained for the TEGBMP-*co*-TAQA, BDBMA-*co*-TAQA, and 1,2-EDT-*co*-TAQA nanocomposites alongside the storage moduli of cancellous and cortical bone.

Table 4. Maximum E` of poly(thioether-*co*-TAQA) composites

Substrate	E` (MPa)
1,2-EDT-*co*-TAQA, 0% cellulose	72
TEGBMP-*co*-TAQA, 1.0% cellulose	211
BDBMA-*co*-TAQA, 0.5% cellulose	238
Cancellous bone	100-4500[6]
Cortical bone	17000-24000[6]

Though fabrication of a purely organic material capable of matching the mechanical properties of cortical bone remains a significant synthetic challenge, both the TEGBMP-*co*-TAQA and BDBMA-*co*-TAQA composites at the levels of additive content reported above exhibit storage moduli well within the parameters of cancellous bone. Consequently, these materials present a viable and similarly bio-based alternative to PLA-based orthopedic implants while exhibiting a greater degree of tunability to better accommodate the diversity of mechanical properties demonstrated by cancellous bone throughout the human body in a range of patient ages.

Degradation of poly(thioether-*co*-TAQA) network composites

To complete the comparative analysis with the neat poly(thioether-*co*-TAQA) networks and provide an additional basis of comparison with PLA, pucks of TEGBMP-*co*-TAQA, BDBMA-*co*-TAQA, and 1,2-EDT-*co*-TAQA containing 1.0 percent cellulose nanocrystals by weight were

subjected to degradation under approximate physiological conditions, mirroring the conditions employed in the original degradation studies conducted by Link et al.[19] Composites containing 1.0 percent cellulose by weight were selected, as it represents a median level of additive content from the range employed for the thermal and mechanical analyses. Samples were washed, massed, dried under vacuum, and remassed on a weekly basis. The timelines for degradation for each of the three composites are reported below in **Figure 4.**

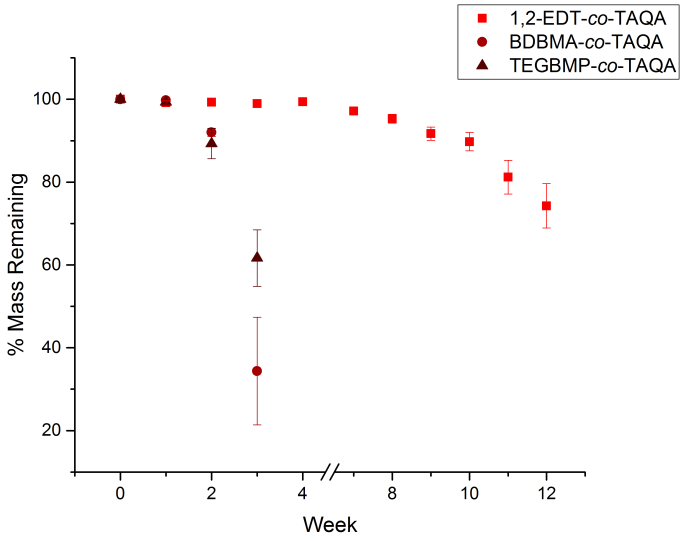

Figure 4. Degradation of poly(thioether-*co*-TAQA) network composites

The patterns of degradation demonstrated differed sharply between the thermoset 1,2-EDT-*co*-TAQA and its elastomeric counterparts, TEGBMP-*co*-TAQA and BDBMA-*co*-TAQA. Composites of 1,2-EDT-*co*-TAQA demonstrated negligible mass loss until week 8, when the first visual signs of surface erosion were observed. The materials continued to decline in mass from weeks 8-12. At week 11, the composites experienced mechanical failure, breaking apart into large pieces in response to light handling; at week 12, those pieces had disintegrated into smaller fragments. By contrast, the TEGBMP-*co*-TAQA and BDBMA-*co*-TAQA composites

began to experience appreciable mass loss in a bulk degradation pattern after two weeks. At this time, the composite materials, originally translucent, became white, opaque, and slightly tacky. In both network systems, this change in color was accompanied by the reappearance of integrated cellulose at the surface of the composites. By week three, the composites of both TEGBMP-*co*-TAQA and BDBMA-*co*-TAQA no longer retained their shape and became sufficiently tacky as to render accurate records of mass challenging, even after the allotted drying period.

While these degradation studies are ongoing, the results obtained thus far permit comparative assessments of the mechanism and timescale of degradation. The poly(thioether-*co*-TAQA) composite materials exhibit degradation patterns (*i.e.*, bulk or surface) that match those of the neat networks; however, the composites degrade at a significantly faster rate than their neat counterparts. This acceleration in degradation rate may be attributed to leaching of the cellulose additive, which would increase water uptake in the polymer matrix and increase the rate of hydrolysis. A second potential contributing factor is the possibility of interference by cellulose crystals during the curing process, which would limit the crosslink density of the resultant network materials, and thus facilitate a more rapid degradation process. To examine this possibility, crosslink densities were calculated for both the neat networks and 1.0 % by weight composites of each of the three poly(thioether-*co*-TAQA) resins examined.

The crosslink density (v_c) of a crosslinked network may be approximated by **Equation 1**.

(1) $$\mathrm{v_c} = \frac{\varepsilon'}{3\mathrm{RT}}$$

where ε' is the rubbery modulus measured at 100°C, R is the ideal gas constant, and T is the temperature. 100°C was selected for these calculations, as all three networks are fully in the rubbery state at that point, ensuring an even point of comparison across all networks.[23] The results of these calculations are reported in **Table 5.**

Table 5. Calculations of ν_c for poly(thioether-*co*-TAQA) neat networks and composites

Network	Cellulose content (% by weight)	ε' (MPa)	ν_c (mol cm^{-3})
TEGBMP-*co*-TAQA	0	1.9	2.03×10^{-4}
TEGBMP-*co*-TAQA	1	2.8	2.97×10^{-4}
BDBMA-*co*-TAQA	0	3.8	4.06×10^{-4}
BDBMA-*co*-TAQA	1	2.2	2.33×10^{-4}
1,2-EDT-*co*-TAQA	0	4.0	4.29×10^{-4}
1,2-EDT-*co*-TAQA	1	2.9	3.15×10^{-4}

As noted above, all networks but TEGBMP-*co*-TAQA demonstrated a decrease in crosslink density with increasing cellulose content. These calculations, coupled with the visual observations of leaching during the degradation study, support the conclusion that a combination of moderated crosslink density coupled with additive leaching is responsible for the accelerated degradation pattern noted for the poly(thioether-*co*-TAQA) network composites.

CHAPTER IV

CONCLUSIONS

The joint pressures of increasing competition for scarce petrochemical resources and sustained demand for engineering polymers with high-performance thermal and mechanical properties have prompted substantial interest in the development of polymers derived from natural products. In the chemical industry, this interest has heralded a major transition of physical resources and capital towards bio-based commodity plastics; in medicine, and most notably in the subspecialty of orthopedics, it has enabled a search for naturally-derived materials that match the thermal and mechanical properties of their petroleum-based counterparts and exceed their capacity to tailor materials to precisely match the demanding requirements of the human body with minimal toxicity.

Recent additions to this growing library include a family of crosslinked polycarbonate networks derived from the natural product quinic acid, found in abundance in coffee and tea. The tunable thermal and mechanical properties and physiologically benign degradation exhibited by these materials rendered them ideally suited to serve as biomedical devices, including temporary orthopedic implants that could be tuned to match the mechanical properties of the surrounding bone and permitted to clear the wound site without significant inflammation or secondary surgical procedures at the conclusion of their useful lives.

To further extend the thermal and mechanical capacities of this family of materials without compromising their physiologically benign mechanisms of degradation, a series of

nanocomposites comprising nanocrystals of cellulose and quinic acid-based poly(thioether-*co*-TAQA) crosslinked networks were devised. A preliminary investigation designed to evaluate the most effective method of additive integration revealed that sonication afforded the greatest degree of additive dispersion, as composites fabricated by this method demonstrated values of T_g up to 10°C higher than those made by other methods of integration. These optimized methods were employed to fabricate TEGBMP-*co*-TAQA, BDBMA-*co*-TAQA, and 1,2-EDT-*co*-TAQA nanocomposites containing up to 7.5 percent cellulose nanocrystals by weight.

Analyses of thermal and mechanical properties conducted by TGA/DSC and DMA, respectively, indicated that increasing levels of cellulose content contributed to modest gains in T_g and variable increases in E` to afford composite materials with glass transition temperatures between -15 and 56°C and storage moduli between 34 and 328 MPa, comparable to cancellous bone. Both thermal and mechanical properties demonstrated substantial variability between samples owing to aggregation of the cellulose nanocrystals in the hydrophobic polymer matrix. Degradation studies conduction under physiological conditions indicated that the composite materials experienced significant degradation between 3 and 12 weeks with mass losses of 25 to 66 percent. While mechanisms of degradation remained consistent between the composite materials and unmodified networks, the composite materials experienced a significantly higher rate of degradation, likely as a result of leaching of the cellulose additive.

In summary, a series of naturally-derived and biodegradable nanocomposites was fabricated. The materials produced augmented the scope of achievable thermal and mechanical properties, presenting a substantial step towards custom orthopedic implants tailored to the mechanical

properties of the surrounding biological environment. Future directions for this investigation will comprise a continuation of the ongoing degradation studies to approach total mass loss and an exploration of potential methods to minimize cellulose aggregation, including surface modification. The surface modification of cellulose has been explored at length in the scientific literature.[24] Acetylation reactions have proven particularly successful in resolving matrix/additive incompatibilities in cellulose-based materials and have recently been employed in the fabrication of reinforced PLA-cellulose composites.[25]

The composite materials fabricated in this study demonstrated promising gains in modulus up to the GPa range and achieved excellent additive dispersion, as evaluated by continuation of optical transparency during melt processing of bulk materials, for composites containing up to 20 percent cellulose by weight. If applied to the poly(thioether-*co*-TAQA) networks, a surface modification strategy towards cellulose integration stands to leverage the burgeoning gains in thermal and mechanical performance described in this work towards the development of a family of highly tunable crosslinked polymer network composites with thermal and mechanical properties valuable for applications within and beyond the fields of biology and medicine.

REFERENCES

1. Coca-Cola Company. An Introduction to PlantBottle Packaging. www.coca-colacompany.com/stories/great-things-come-in-innovative-packaging-an-introduction-to-plantbottle-packaging/ (accessed May 2, 2016).

2. Scott, A. Lego To Replace Oil-Based Plastics *C&EN* [Online], 2015. http://cen.acs.org/articles/93/i26/Lego-Replace-Oil-Based-Plastics.html (accessed September 5, 2016).

3. Synvina: Joint venture of BASF and Avantium established. https://www.basf.com/en/company/news-and-media/news-releases/2016/10/p-16-322.html (accessed March 19, 2017).

4. Pasco, J.; Lane, S.; Brennan-Olsen, S.; Holloway, K.; Timney, E.; Bucki-Smith, G.; Morse, A.; Dobbins, A.; Williams, L.; Hyde, N.; Kotowicz, M. *Calcif. Tissue Int.* **2015**, 1-9.

5. Hoppenfeld, S.; Murthy, V. L., *Treatment & Rehabilitation of Fractures*. Lippincott Williams & Wilkins: Philadelphia, 2000.

6. Middleton, J. C.; Tipton, A. J. *Biomaterials* **2000,** *21*, 2335-2346.

7. Persons, B. L.; Wong, G. B., Transantral endoscopic orbital floor repair using resorbable plate. *J. Craniofac. Surg.* **2002,** *13*, 483-388.

8. Lopes, M. S.; Jardini, A. L.; Filho, R. M. *Proc. Eng.* **2012,** *42*, 1402-1413.

9. Miller, S. A. *ACS Macro Lett.* **2013,** *2*, 550-554.

10. Link, L. A.; Lonnecker, A. T.; Hearon, K.; Maher, C. A.; Raymond, J. E.; Wooley, K. L. *ACS Appl. Mater. Interfaces* **2014,** *6*, 17370-17375.

11. Hauenstein, O.; Agarwal, S.; Greiner, A. *Nat. Comm.* **2016,** *7*, 11862.

12. Noel, A.; Borguet, Y. P.; Raymond, J. E.; Wooley, K. L. *Macromolecules* **2014,** *47*, 2974-2983.

13. Galbis, J. A.; García-Martín, M. d. G.; de Paz, M. V.; Galbis, E. *Chem. Rev.* **2016,** *116*, 1600-1636.

14. Kristufek, S. L.; Yang, G.; Link, L. A.; Rohde, B. J.; Robertson, M. L.; Wooley, K. L. *ChemSusChem* **2016,** *9*, 2135-2142.

15. Clifford, M. N. *J. Sci. Food Agric.* **2000,** *80*, 1033-1043.

16. Besset, C. J.; Lonnecker, A. T.; Streff, J. M.; Wooley, K. L. *Biomacromolecules* **2011,** *12*, 2512-2517.

17. Garg, N. K.; Caspi, D. D.; Stoltz, B. M. *J. Am. Chem. Soc.* **2004,** *126*, 9552-9553.

18. Capadona, J. R.; Shanmuganathan, K.; Trittschuh, S.; Seidel, S.; Rowan, S. J.; Weder, C., *Biomacromolecules* **2009,** *10*, 712-716.

19. Link, L. A. Degradable Polycarbonate Networks Derived from Quinic Acid and Designed for Biomedical Applications. Ph.D. Thesis, Texas A&M University, October 2015.

20. *Select Committee on GRAS Substances (SCOGS) Opinion: Cellulose and Microcrystalline Cellulose*. United States Food & Drug Administration: Washington, DC, 1973.

21. Herrera, N.; Mathew, A. P.; Oksman, K. *Compos. Sci. Technol.* **2015,** *106*, 149-155.

22. Houdas, Y.; Ring, E. F. J., *Human Body Temperature: Its Measurement and Regulation*. Springer Science & Business Media: New York, 1982.

23. Hill, L. W., *Prog Org. Coat.* **1997,** *31*, 235-243.

24. Eyley, S.; Thielemans, W. *Nanoscale* **2014,** *14*, 7764-7779.

25. Braun, B.; Dorgan, J. R.; Hollingsworth, L. O. *Biomacromolecules* **2012,** *13*, 2013-2019.

APPENDIX: PHOSGENE-FREE SYNTHESIS OF POLY(TYROSOL CARBONATES)

CHAPTER I

INTRODUCTION

A combination of solvent resistance, mechanical robustness, and optical clarity render polycarbonates well-equipped for a variety of applications in both consumer goods and high-performance materials.[1] High demand for these polymers, coupled with recent scrutiny over potential safety issues associated with the use of bisphenol A (BPA) polycarbonate in consumer and patient contact applications[2-3] has resulted in considerable demand for biocompatible and bio-based alternatives. Recent efforts towards the synthesis of these bio-based polycarbonates have included materials derived from limonene,[4] honokiol,[5] and guanosine.[6]

To expand this growing library of natural product precursors for engineering polymers, the focus of investigation shifted to tyrosol, a phenol found in abundance in olive oil and wine that demonstrates the ability to limit radical oxidation of cholesterol, a contributing factor in heart disease.[7] To date, tyrosol has been employed as a natural precursor in the synthesis of linear[8] and brush[9] polymethacrylates and high tensile strength polycarbonates both independently[10] and as a comonomer with homovanillyl alcohol.[11] However, these existing polymerizations require the use of triphosgene, which produces the highly efficient and highly toxic reagent phosgene *in situ*, creating a potential safety hazard. To advance this body of work, a novel synthetic strategy towards linear poly(tyrosol carbonates) was devised to eliminate dependence on the highly toxic

reagent phosgene and introduce a fundamental study of regioregularity and its influence on thermomechanical properties.

CHAPTER II

METHODS

Materials & Characterization

Materials

Acetonitrile (Sure-Seal), *tert*-butyldimethylsilylchloride (TBDMSCl), and tyrosol were obtained from Sigma Aldrich. Sodium hydride (NaH, 60% dispersion in mineral oil) was obtained from Acros Organic. Silver fluoride (AgF) and imidazole were purchased from Alfa Aesar. Anhydrous solvents (DCM, DMF, THF) were obtained by in-house solvent purification system (SPS).

Characterization

^{1}H and ^{13}C nuclear magnetic resonance (NMR) spectra were obtained on a Mercury 300 spectrometer interfaced to a UNIX computer with VnmrJ software. Chemical shifts were referenced to the appropriate solvent (CD_3OD: 3.31, $CDCl_3$: 7.26 ppm). Infrared (IR) spectra were obtained on a Shimadzu IR Prestige system and analyzed by IResolution software. Gel permeation chromatography (GPC) was completed on a Waters isocratic pump (model 1515) equipped with an inline degasser, differential refractometer (model 2414) calibrated with polystyrene standards (Polymer Laboratories, 300-467,000 Da), and a series of four Styragel columns obtained from Polymer Laboratories, Inc. (PL_{gel} 5 μm guard column, 50 x 7.5 mm; PL_{gel} 5 μm Mixed C, 300 x 7.5 mm; PL_{gel} 500 Å, 300 x 7.5 mm; PL_{gel} 10^4 Å, 300 x 7.5 mm). Polymer samples were prepared as solutions in N, N-dimethylformamide (DMF) with approximate

concentration of 3 mg/mL and total injection volume of 200 μL. Toluene (0.05 % by volume) was employed as a flow rate marker.

Methods

Synthesis of 4-(2-((tert-butyldimethylsilyl)oxy)ethyl)phenol

To an oven-dried 250 mL flask equipped with a stir bar, tyrosol (4.5018 g, 32.5840 mmol), imidazole (4.5457 g, 66.7704 mmol) and 133 mL anhydrous dimethylformamide (DMF) were added. The flask was purged and placed under nitrogen; a solution of TBDMSCl (5.420 g, 35.9607 mmol) in 22 mL of anhydrous DMF was then added dropwise over 30 minutes, stirring vigorously. The mixture was allowed to react for 19 h, monitored by TLC. The reaction mixture was then concentrated by high-vacuum rotary evaporation to a crude oil, which was partitioned with 100 mL of diethyl ether and 50 mL of HCl (2 N, pH 4). The aqueous layer was extracted a second time against 15 mL diethyl ether; the organic extracts were then combined and washed with 50 mL of brine. The resulting organic layer was dried over $MgSO_4$ and concentrated to afford a white crystals, which were dissolved in 20 mL of hexanes and passed through a silica plug to afford the intended product in fair yield (2.9787 g, 40% yield). ^{1}H NMR ($CDCl_3$, 300 MHz): δ 7.07 ppm, (d, J=7.1, 2 H, H-3, H-5), 6.76 ppm (d, J=6.8, 2 H, H-2, H-6), 3.76 ppm (t, J=3.8, 2 H, H-8), 2.75 ppm (t, J=2.8, 2 H, H-7), 0.88 ppm (s, 3 H, H-11, H-13, H-14), 0.01 ppm (s, 2 H, H-9, H-10). FTIR (neat, cm^{-1}): 3260, 2934, 2857, 1516, 1078. LRMS (ESI-TOF) m/z: [M + Na] Predicted: 275.14 Found 275.07.

Synthesis of 4-(2-((tert-butyldimethylsilyl)oxy)ethyl)phenyl 1H-imidazole-1-carboxylate

To an oven-dried 100 mL round-bottom flask, 30 mL of THF were added. The flask was then cooled to 0°C and NaH (60% dispersion in mineral oil, 0.2256 g, 9.4009 mmol) was added. A solid addition funnel containing CDI (2.7590 g, 17.0151 mmol) was attached; the apparatus was then purged and placed under nitrogen. A solution of 4-(2-((tert-butyldimethylsilyl)oxy)ethyl)phenol (1.4929 g, 5.9141 mmol) in 6 mL of THF was then added dropwise through the straight sidearm of the addition funnel and allowed to react for 5 minutes. CDI was added at a slow, constant rate from the addition funnel over 50 minutes. The mixture was then allowed to react for three hours, monitored by TLC. Once complete, the reaction mixture was filtered through a medium-pore fritted funnel and washed with THF. The solvent was removed to afford off-white crystals, which were washed with 50 mL of hexanes. The filtrate remaining after the washes was then concentrated to afford the intended product as a colorless oil in good yield (1.5899 g, 78%). ^{1}H NMR ($CDCl_3$, 300 MHz): δ 8.29 ppm (s, 1 H, H-14), 7.56 ppm (s, 1 H, H-12), 7.30-7.27 ppm (d, J=7.3, 2 H, H-2, H-3), 7.17-7.15 ppm (d, J=7.2, 3 H, H-1, H-4, H-13), 3.84-3.79 ppm (t, J=3.8, 2 H, H-6), 2.86-2.82 ppm (t, J=2.8, 2 H, H-5), 0.86 ppm (s, 9 H, H-9-H-11), 0.02 ppm (s, 6 H, H-7, H-8). FTIR (neat, cm^{-1}): 2928, 2857, 1776, 1383, 1242.

Polymerization of 4-(2-((tert-butyldimethylsilyl)oxy)ethyl)phenyl 1H-imidazole-1-carboxylate

To an oven-dried 10 mL Sclenk flask equipped with a stir bar and wrapped in foil, the difunctional tyrosol monomer was added (0.0977 g, 0.2802 mmol). The flask was purged and placed under nitrogen; 1.5 mL of Dry-Solv acetonitrile was then added. AgF (0.0831 g, 0.6550 mmol) was added in a darkened room. The flask was quickly purged a second time; nitrogen

flow was then restored for the duration of the reaction. The reaction mixture was heated to 45 °C; polymerization was allowed to continue. An aliquot (0.3 mL) was retrieved for analysis at 24 h. The solution appeared amber in color and was quenched in 20 mL of wet methanol (10% water v/v) to afford a cloudy white precipitate. The quenched solution was spun down by centrifuge at 8500 rpm for 10 minutes to afford a thin white film on the side of the vial employed. The supernatant liquid was decanted. Attempts to retrieve the film from the vial were unsuccessful. Consequently, the polymer was dissolved in 10 mL DCM, transferred to a 25 mL round-bottom flask, and concentrated to reestablish a thin film of polymer. This film was dissolved in 2 mL of DMF; a small fraction (0.2 mL) of this solution was filtered and subsequently analyzed by gel permeation chromatography (GPC) using DMF as the eluent. Analysis revealed a peak corresponding to the polymer at 23 minutes of elution time. M_n = 19 kDa, M_w = 63 kDa, Đ = 3.3, DP = 117.

CHAPTER III

RESULTS & DISCUSSION

Synthetic design

The proposed synthetic strategy towards phosgene-free poly(tyrosol carbonates) entailed a two-step monomer synthesis, followed by a polycondensation initiated by AgF.

Scheme 1. Synthetic route towards poly(tyrosol carbonates)

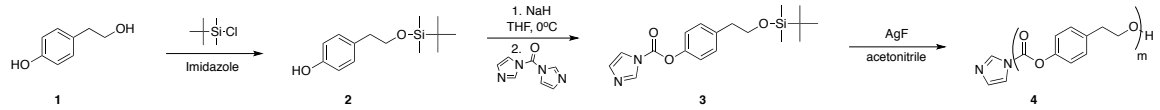

This approach is based on the differing reactivities of the two hydroxyl functionalities present on tyrosol (**1**). By adapting the reagents employed to selectively functionalize each group, a difunctional monomer amenable to phosgene-free polymerization could be obtained. The synthetic route towards this monomer was adapted from chemistry previously employed in the formation of hyperbranched aromatic polycarbonates.[12] From tyrosol (**1**), the synthesis begins with protection of the hydroxyl group by tert-butyldimethylsilyl chloride (TBDMSCl).

Scheme 2. Synthesis of 2-protected pre-monomer

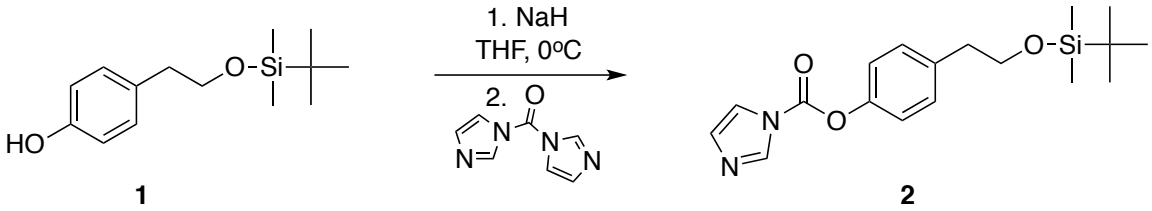

Literature indicates that sequential treatment of tyrosol with imidazole and TBDMSCl will afford **2** through a general base pathway.[13] Imidazole is a comparatively weak base and insufficiently strong to deprotonate the phenolic hydroxyl group, leaving the primary alcohol as the primary

reactive site for TBDMSCl. Once protected, the exposed phenol on **2** will then undergo deprotonation with NaH and subsequent addition of 1,1'-carbonyldiimidazole to afford the A-B monomer **3**.

Scheme 2. Synthesis of 2-, 4-protected monomer

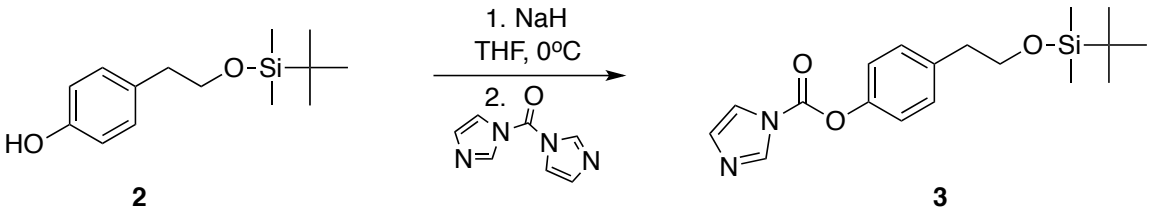

2 **3**

Reaction with excess AgF will remove the TBDMS protecting group, enabling a polycondensation reaction driven towards conversion to the poly(tyrosol carbonate) **4** by the continuous formation of insoluble silver imidazole salts.

Scheme 3. Polymerization of the 2-,4-functionalized monomer

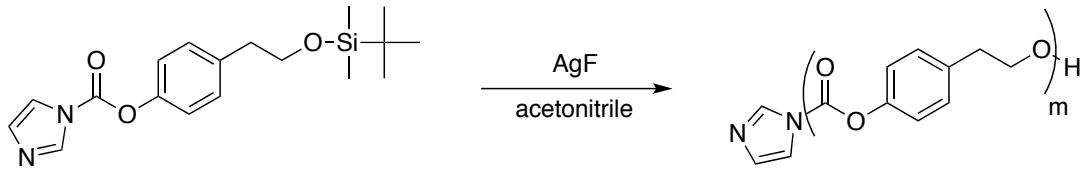

3 **4**

Pre-monomer synthesis

To begin the synthesis of the difunctional tyrosol monomer, the pre-monomer 4-(2-((tert-butyldimethylsilyl)oxy)ethyl)phenol was first prepared.[13] In this reaction, the silicon present in TBDMSCl was complexed to the oxygen of the primary alcohol present on **1**. Imidazole enabled the subsequent removal of the chloride from TBDMSCl, enabling formation of a highly stable Si-O bond to afford **2.** This synthesis was first attempted in DMF, as directed in the literature, and then in THF and in DCM. The results of these attempts are summarized below in **Table 1.**

Table 1. Synthesis of tyrosol pre-monomer

Solvent	Temperature (°C)	Imidazole (eq.)	TBDMSCl (eq.)	Reaction time (h)	Yield (%)
DCM	25	2.1	1.1	19	39
THF	25	2.1	1.1	19	39
DMF	25	2.1	1.1	19	60
DMF*	25	2.1	1.1	19	40

* Column-free workup

DMF afforded the highest yields of **2**, with 60% yield, whereas syntheses in both DCM and THF afforded 40%. The intended product was obtained in good purity, as measured by ^{1}H NMR, where the appearance of singlet peaks at 0.88 and 0.00 corresponding to the *tert*-butyl and methyl groups, respectively, supports the successful formation of the intended product. In further support of the success of this synthesis, MS afforded a mass of 275.07, in good agreement with the predicted mass of 275.12.

Of note, all three solvent systems employed afforded **2** in high selectivity; neither monitoring by TLC nor analysis of crude products by NMR noted appreciable formation of phenol-protected or diprotected byproducts. With the synthesis optimized for solvent conditions, focus shifted to minimizing the environmental impact associated with the reaction. To do so, the reaction was again attempted in DMF, the highest-yielding solvent, but was purified by passage through a silica plug in lieu of the LCMS column, as suggested by the literature. This substitution was possible because the starting material, **1**, does not elute readily in a hexanes/ethyl acetate mixture. While the yield decreased appreciably with this substitution, the volume of solvent expended in the workup declined significantly. Moreover, with minor optimization, the yield of reactions employing this alternative workup method may be improved to levels comparable with established procedures.

Monomer synthesis

To complete the synthesis of the monomer, 4-(2-((tert-butyldimethylsilyl)oxy)ethyl)phenyl 1H-imidazole-1-carboxylate, a carbonylimidazole moiety was installed by sequential deprotonation of **2** with NaH and addition of CDI. Procedures for this reaction were adapted from the synthesis of a structurally similar singly functionalized small molecule in the literature.[12] The results of this synthesis and its subsequent optimization are reported in **Table 2.**

Table 2. Synthesis of tyrosol monomer

Solvent	Temperature (°C)	NaH (eq.)	CDI (eq.)	Reaction time (h)	Yield (%)
THF	0	1.5	2.9	2	NC
THF	0	1.5	3.6	2	23
THF	0	1.5	5.8	2	24
THF	0	2.1	2.9	3	30
THF	0	1.5	2.9	3	78

After an initial attempt at the synthesis afforded no conversion of **2**, the excess of CDI was increased first to 3.6, and then to 5.8 equivalents. However, these attempts afforded relatively low yield. Subsequently, the amount of CDI was restored to literature conditions and the excess of NaH was increased, as well as the reaction time. When these modifications garned only minor improvements in yield with full conversion noted by TLC and no detectable amounts of product lost either during aqueous washes or drying steps, the column chromatography procedure employed was examined in closer detail. Completion of a two-dimensional TLC test, coupled with a thorough review of the column traces obtained during previous reactions revealed that the persistent low yields could be attributed to the rapid decomposition of **3** on silica.

Consequently, the installation of the carbonylimidazolide functionality was attempted again under the original literature conditions with a substantially modified workup. In place of concentrating, washing with DCM and sodium carbonate and purifying by column

chromatography, the crude reaction mixture was concentrated and the resultant solids washed with approximately 50 mL of hexanes. The resultant filtrate was concentrated to afford **3** as a colorless oil with 78% yield, a nearly fourfold improvement over previous attempts. ^{1}H NMR and FTIR were again performed to support the successful synthesis of the monomer. The continued presence of the NMR peaks around 0.88 and 0.00 demonstrates that the addition of NaH was not sufficient to remove the TBDMS protecting group, and the appearance of characteristic singlet peaks at 8.29 and 7.56 corresponding to protons of the imidazole ring closest to the carbonyl indicates that the carbonylimidazolide moiety was successfully installed. The FTIR spectra of the pre-monomer and monomer, which clearly notet he disappearance of the phenolic OH peak at 3260 and appearance of the C=O stretch at 1776, as seen in **Figure 1**, further support this assertion.

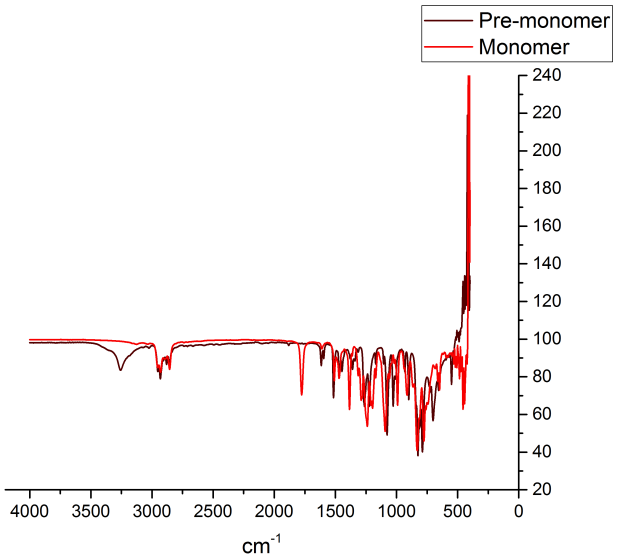

Figure 1. Overlay of FTIR spectra of tyrosol pre-monomer and monomer

The modifications to the workup of the monomer synthesis are of particular significance, as they suggest that the full synthesis of the difunctional monomer may be performed from a biobased

monomer and without the use of column chromatography. This dramatically reduces the amount of solvent waste associated with the chosen synthetic design, thus improving its sustainability.

Synthesis of poly(tyrosol carbonate)

With both pre-monomer and monomer syntheses optimized, the polymerization of **2** to afford a linear poly(tyrosol carbonate) was undertaken. Working from a procedure originally developed for the synthesis of hyperbranched polycarbonates by Bolton & Wooley[12], the polymerization was completed on a small, 100 mg scale to serve as a proof of concept for the proposed phosgene-free strategy. As discussed previously, the reaction is initiated by AgF, wherein the fluoride anion cleaves the TBDMS functionality to afford TBDMSF salts and an exposed alkoxy group. This alkoxy group may then subsequently attack the carbonylimidazolide moiety on a second monomer to establish the carbonate linkage characteristic of a polycarbonate. The polymerization is driven towards further conversion by the precipitation of silver imidazole salts, which drive the equilibrium of the reaction towards product formation. The resulting poly(tyrosol carbonate) was precipitated in MeOH, with some difficulty, and subsequently analyzed by gel permeation chromatography (GPC). The GPC trace, depicted below in **Figure 2**, indicates successful formation of the polymer by a peak at 23 minutes of elution time.

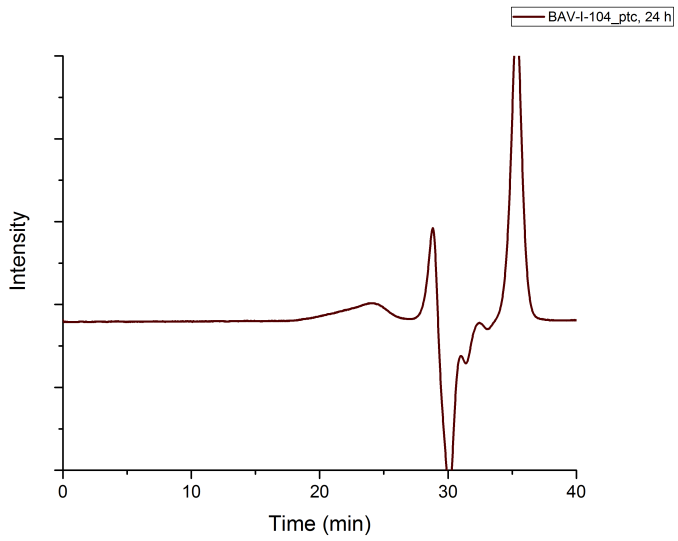

Figure 2. GPC trace of poly(tyrosol carbonate)

Quantitative results of the GPC analysis, are presented in **Table 3**, where M_n is the number-average molecular weight, M_w is the weight-average molecular weight, Đ is the polydispersity, calculated as the ratio of M_w to M_n, and DP is the degree of polymerization, or the number of repeat units.[1]

Table 3. Characterization of poly(tyrosol carbonate)

Reaction time (h)	M_n (kDa)	M_w (kDa)	Đ	DP
24	19	63	3.3	117

With a M_n of 19 kDa and DP of 117 after only 24 hours, this test polymerization indicates that phosgene-free synthesis of poly(tyrosol carbonates) is well within the realm of possibility and offers substantial promise for scale-up and exploration of the relationship between chain length and reaction conditions, both of which are ongoing at present.

CHAPTER IV

CONCLUSIONS

In summary, high demand for polycarbonates from a variety of industries and growing concern over both sustainability and safety have prompted a proliferation in naturally-derived polycarbonates. To contribute to the growing library of bio-based polycarbonates and improve the safety and efficacy of existing efforts, tyrosol, a phenolic compound found in olive oil, was employed as a natural product precursor in the column-free synthesis of a difunctional monomer that was subsequently employed in a phosgene-free polycondensation to afford linear poly(tyrosol carbonates) with substantial promise as bio-based engineering materials.

Future directions for this work entail a continuation of the fundamental study introduced above, as well as a thorough analysis of the thermal and mechanical properties of these materials, particularly with respect to "industry standard" polymers, including BPA polycarbonate and poly(terephthalic acid), or PET. Finally, cytotoxicity assays will be performed to assess the biocompatibility of these poly(tyrosol carbonates) and evaluate their suitability for potential applications in biology and medicine.

REFERENCES

1. Hiemenz, P. C.; Lodge, T. P., *Polymer Chemistry*. 2nd ed.; CRC Press: Boca Raton, 2007.

2. Vandenberg, L. N.; Maffini, M. V.; Sonnenschein, C.; Rubin, B. S.; Soto, A. M. *Endocr. Rev.* **2009,** *30*, 75-95.

3. *Opinion on the safety of the use of bisphenol A in medical devices.* European Commission Scientific Committee on Emerging and Newly Identified Health Risks: 2015; pp 1-129.

4. Hauenstein, O.; Agarwal, S.; Greiner, A. *Nat. Comm.* **2016,** *7*, 11862.

5. Wacker, K. T.; Kristufek, S. L.; Lim, S.-M.; Kahn, S.; Wooley, K. L. *RSC Adv* **2016,** *6*, 81672-81679

6. Gregory, G. L.; Hierons, E. M.; Kociok-Kohn, G.; Sharma, R. I.; Buchard, A. *Polym. Chem.* **2017,** *8*, 1714-1721

7. Miro-Casas, E.; Covas, M. I.; Fito, M.; Farre-Albadalejo, M.; Marrugat, J.; de la Torre, R. *Eur. J. Clin. Nutr.* **2003,** *57*, 186-190.

8. Tsuchiya, K.; Endo, T. *J. Polym. Sci. Part A: Polym. Chem.* **2014,** *52*, 699-706.

9. Ohno, K.; Akashi, T.; Tsujii, Y.; Yamamoto, M.; Tabata, Y. *Biomacromolecules* **2012,** *13*, 927-936.

10. Kohn, J. B.; Bolikal, D. U. S. Patent 9,416,090, 2013.

11. Sommerfeld, S. D.; Zhang, Z.; Costache, M. C.; Vega, S. L.; Kohn, J. *Biomacromolecules* **2014,** *15*, 830-836.

12. Bolton, D. H.; Wooley, K. L. *Macromolecules* **1997,** *30*, 1890-1896.

13. Box, P.; Coe, D.; Looker, B.; Procopiou, P. U.S. Patent 2005256201, 2005.